International Journal of Mechanical and Production Engineering Research and Development (IJMPERD)
ISSN(P): 2249-6890; ISSN(E): 2249-8001
Vol. 9, Issue 3, Jun 2019, 839-854

Original Article

A COMPARATIVE ASSESSMENT OF TENSILE STRENGTH AND CORROSION PROTECTION IN FRICTION STIR PROCESSED AA7075-T651 MATRIX COMPOSITES USING FLY ASHES NANOPARTICLES AS REINFORCEMENT INHIBITORS IN 3.5 % NaCl

OMOLAYO M. IKUMAPAYI[1*] & ESTHER T. AKINLABI[1,2]

[1]*Department of Mechanical Engineering Science, University of Johannesburg, Auckland Park Kingsway Campus, Johannesburg, South Africa*

[2]*Department of Mechanical Engineering, Covenant University, Ota, Nigeria*

ABSTRACT

This research presents the performance of eco-friendly waste materials, which are wood fly ash nanoparticle (WFA-NPs) and coal fly ash nanoparticles (CFA-NPs) as economical reinforcements corrosion inhibitors on friction stir processed Aluminium 7075-T651 alloy in 3.5 % NaCl solution at room temperature and at a stable pH of 7. This study investigated the tendency of using domestic waste wood fly ash and industrial waste coal fly ash as a promising and potential alternative to metallic powders for reinforcements and corrosion mitigation in friction stir processed (FSP)armour grade aluminium 7075-T651 alloy and at the same time compare their efficacy. Microchannel of 3.5 mm depth and 2.0 mm width was machined on each aluminium plate with the aid of horizontal milling machine to deposit fly ashes (FAs) nanoparticles. Optimum process parameters chosen for the FSP experimentation are processing speed, rotational speed, tool tilt angle and plunging depth which were 20 mm/min, 1500 rpm, 3 ° and 0.3 mm respectively. Two passes on each parameter with 100 % inter-pass overlap was achieved. A cutting tool with a tapered cylindrical pin profile made of AISI H13 steel tool was employed for FSP with a shoulder diameter of 18 mm, pin diameter of 5 mm and a pin length of 5 mm. In this study, the tensile strength was investigated using X force P type of Zwick/Roell Z250 tensile testing machine with a normal force of 250 KN and characteristic of 2mV/v. It was revealed that unprocessed and untreated base metal (UBM) has the highest values for ultimate tensile strength which were 620.9030 MPa and its breaking force was 22.35252 KN with an elastic modulus of 9.38165 GPa. There was no significant improvement in tensile strength properties when processed and or reinforced with either WFA-NPs or CFA-NPs. In contrast, there was tremendous and excellent improvement in corrosion protection ability of calcined WFA-NPs as against CFA-NPs when applied as reinforcement inhibitor which lead to reduction in corrosion rate from 5.0718 to 0.12068 mm/year with the highest percentage corrosion inhibitive performance efficiency (%IPE) from 63.9 % on reinforced to 97.61 % reinforced with WFA-NPs.

KEYWORDS: Corrosion Rate, Coal Fly Ash, Wood Fly Ash, Tensile Strength & Friction Stir Processing

Received: Feb 10, 2019; **Accepted:** Mar 04, 2019; **Published:** May 16, 2019; **Paper Id.:** IJMPERDJUN201992

INTRODUCTION

Many researchers in recent years and nowadays have investigated the tensile strength and the corrosion behaviours of AA7075 at different tapered conditions using different approaches varying from using different second phases as reinforcement particles and corrosion inhibitors at different concentrations of seawater and other

medium in order to exploit the tensile strength and corrosion mitigation efficiency to using numerical simulation approaches to predict the strength and corrosion protection of AA7075. In this study, wood and coal fly ashes nanoparticleshave been used as reinforcement particles and corrosion inhibition in friction stir processed aluminium alloy 7075-T651 using 3.5 % NaCl solution as seawater corrosive environmental medium.

Aluminium alloys in general especially commercials available rolled sheet, amour grade, high strength alloy such as 7075 series has gained promising interest as part of the components for defensive equipment. Its areas of applications including the following in defence technologies but not limited to the jet engine, ballistic, space and air vehicles, aviation, military armour tank, fighter aircraft[1]–[3]. Other applications can be traced to automotive, electrical, tribological, thermal structures, shipbuilding and also cryogenic areas of usage in order to optimise fuel consumption in transportation industry and many more due to its exceptional, excellent and unbeatable combination and integration of mechanical, chemical, structural as well as metallurgical properties such as good corrosion resistance, high strength-to-weight ratio, low coefficient thermal expansion, high specific stiffness and strength, oxidation and wear resistance, high plastic flow strength, high thermal and electrical conductivity, high fatigue strength, superior damping capacities, creep resistance, etc. [4], [5].

Friction stir processing is a promising and a novel processing techniques derived from Friction Stir Welding (FSW) whereby a groove (microchannel) that will house the second phase (reinforcement particles) may be created or may not be created on the substrate [6], [7]. FSP has been used widely in many industries today to modify the mechanical properties and surface integrity of the workpiece. It is facile and economical, update and cost-effectiveto using FSP in the preparation of aluminium metal matrix composites[8], [9]. Lots of benefits attributed to the use of FSP amongst which are the homogeneity of the processed zone, homogenization of precipitates, grain refinement, densification of aluminium alloys and composites materials [10]. FSP is a new technology for surface properties improvement of the alloy metals, hardness, ductility, formability improvements and also to enhance the strength of the metal and elongate the fatigue life without any alteration to the properties of the bulk metal [11]. In order to improve the surface quality by FSP, some challenges are encountered during the process of reinforcing the composite materials such as tool wear, sticking of the substrate to the backing plate especially when the job is in thickness between 1mm to 2mm, challenge on how to improve fatigue property and joining strength, many optimizations may be required to obtain optimum parameters and this may lead to the usage of many materials[12]–[15].

Friction stir processing (FSP) for the fabrication of composites be it matrix or hybrid has gotten the attention of researchers nowadays. In order to optimise and validate the potency of reinforcement particulates on electrochemical, metallurgical, and mechanical properties, several characterisations had been carried out. Surface integrity of aluminium alloy 7075 and 6061 were investigated using Boron Carbide powder (B4C). Their hardness, wear and mechanical properties were evaluated after fabricated using friction stir processing. It was revealed that more homogeneous dispersion were seen in the fabricated AA6061/B4C than AA7075/B4C. It was then concluded that fine particles may tend to disperse in AA7075 than when they are not in fine particle [16].

Wear behaviour of friction stir processed Al7075-T651 aluminium alloy using SiC reinforcement was investigated. The processing parameters were at a constant rotational speed of 710 rpm with a varying processing speed of 20, 40 and 56 mm/min. The wear behaviour was carried out using ball-on-disk configuration techniques with normal loads of 2, 4 and 5 N and a linear speed of 2.5 cm/s. A metallographic investigation such as SEM-EDX was carried out on the

wear samples and it was revealed that under 2N normal load, there exist better wear properties, even though, there was a reduction in average hardness of the SiC processed samples[17]. Dry sliding behaviour of friction stir processed of Aluminium alloy AA7075/ZrB2 matrix composites was studied. The particle sizes of the reinforcement phases were between 5–15 % by weight and the applied loads were between 20 – 80 N with varying sling speed of 0.8 – 2.0 m/s at a constant sliding speed of 3000 m. Formation of oxide rich tribolayer in the worn surface led to a reduction of COF. It was revealed that increase in reinforcement particles leads to an increase in hardness of the matrix composites[18].

MATERIALS AND METHODS

Commercially available amour grade aluminium 7075-T651 alloy plates of thickness 6 mm was employed as the base material (substrate) in this study. The plates were dimensioned to have a length of 300 mm and a breadth of 125 mm (i. e. 300 x 125 x 6 mm^3). The spark spectrometry was carried out on the base material – Aluminium Alloy 7075 – T651 and the result is furnished in Table 1 and the various mechanical properties of AA7075 – T65, namely hardness, young modulus, tensile, fatigue, elongation etc. are presented in Table 2.

Table 1: Chemical Composition AA7075-T651 Aluminium Alloy

Elements	Mg	Fe	Ti	Si	Mn	Zn	Cu	Cr	Al
Wt.% Composition	2.8	0.15	0.02	0.05	0.01	5.92	1.93	0.193	**Bal**

Table 2: Mechanical Properties AA7475 – T651

Properties	Value
Fatigue Strength	160 MPa
Ultimate Tensile Strength (UTS)	570 MPa
Elongation at Break	8.2 %
Shear Strength	330 MPa
Brinell Hardness	150
Poisson's Ratio	0.32
Elastic Modulus (Young's, Tensile)	70 GPa
Yield Strength	500 MPa
Shear Modulus	26 GPa

Reinforcement and Inhibitive Materials Collection and Preparations

Coal Fly Ash (CFA) and Wood Fly Ash (WFA) are the major reinforcement particles used in this study. Each particle was obtained in their micro level and then undergone a milling process for 60 minutes to obtain nanoparticle using a vibratory disc milling machine. The CFA was collected at ESKOM coal power station located at Majuba, Mpumalanga province of South Africa while the WFA was collected from the complete combustion of bunches of firewood. After the collection of the two fly ashes (FA), they were sieved, washed with de-ionized water to remove contaminants and impurities that may be present within, the water was then drained and the FAs were then dried at ambient temperature for 72 hours, after which it was then dried further inside an electric oven set at 80 °C for further 48 hours, this is to ensure complete dryness before characterization. After oven dried, the FAs were then sieved using ASTM meshes standard made of King Test Sieve Shaker (VB 200/300), the initial sieving was taken at a 75µm size which was taken to be 0 min milled, after which progressive milling took place for 20, 40 and 60 minutes. Nanoparticles were said to be achieved at 60 minutes milled and the characterizations of the Wood fly ash nanoparticle (WFA-NPs) and coal fly ash nanoparticle (CFA-NPs) were then carried out. The flowchart for the preparations and characterizations of fly ashes is shown in Figure 1.

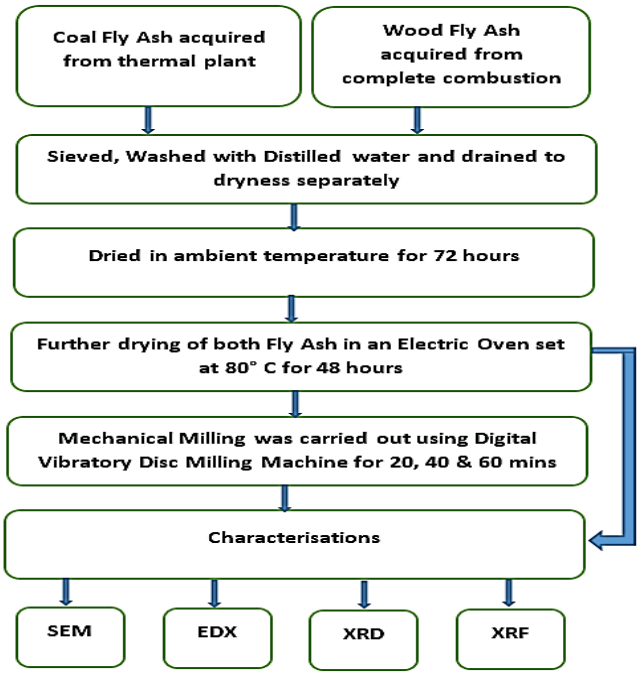

Figure 1: Schematic Diagram for the Preparation and Characterizations of CFA & WFA

Method of Conditioning Wood and Coal Fly Ashes Nanoparticles

Calcination process is process or method of heating a substance with controlled temperature and controlled environment, i. e. thermal treatment process of material in the absence or limited supply of air in order to induce thermal stability, phase transition, thermal decomposition as well as the removal of a volatile fraction from the material before using. This is done to improve the strength, texture, thermal stability etc. The milled FAs nanoparticles cannot be applied directly as reinforcement to the workpiece that will be processed without first of all conditioned to a stable temperature to remove the impurities and contaminants that may be trapped within. On this note, the processed powders were first undergone calcination, which is, conditioning process to ensure thermal stability. The calcination of each powder was carried out by putting each WFA-NPs and CFA-NPs in a separate pure graphite crucible and then put them carefully inside the muffle furnace set at 500 $^{\circ}$C one after the other for two (2) hours, after the 2 hours the furnace was put off and the carbonaceous powder was allowed to cool to room temperature inside the furnace before it was brought out for use and then further ground was performed on each powder to ensure smoothness of the carbonaceous powder before use.

EXPERIMENTAL PROCEDURES USED IN FRICTION STIR PROCESSING

Friction stir processing (FSP) was carried out on a two Ton linear numerical controlled friction stir welding (FSW) machine produced by ETA Bangalore, India Ltd as shown in Figure 2a, the machine is equipped with a load cell that is responsible to take forces along the Z direction. The schematic representation of the arrangement is shown in Figure 2b. The machine has several embedded sensors that are capable of recording velocities x-axis, z – position, x- position of the tool, and x – load etc. The machine has a Lab View software features capable of acquiring real-time data. The recorded and stored vertical axis loads were then extracted and used for the processing. During FSP, aluminium 7075-T651 alloy plate is position in such a way that advancing side (AS) will be positioned along the tool clockwise rotation, that is, the side at which plasticized material is drawn by the tool shoulder while the retreating side (RS) will be positioned in reverse

side which consolidate the material. The location of advancing and retreating sides depend upon the direction of the tool rotation and the tool traverse direction. Figure 2c shows the schematic representation of AS and RS as the tool rotates clock-wisely and also the placement of pressure plate on the workpiece to enable rigid clamping and at the same time proper and rigorous stirring for effective mixing of the materials through the tool pin penetration and the interaction of the shoulder with the workpiece via the tool translational and rotational. The grooves on the Al-plates were created by a horizontal milling machine and the microchannel has 3.5 mm depth and 2.0 mm width for 280 mm long. Both the WFA-NPs and WFA-NPs were packed separately on the plates and pinless tool (See Figure 2d) of 18 mm shoulder diameter made of AISI H13 tool steel was employed to compact the powder and cover up the opening of the groove. After all, a cylindrical tapered tool as shown in Figure 2e made of AISI H13 tool steel of shoulder diameter 18 mm, pin diameter 5 mm and the pin length of 5 mm with 10° taper was used for material stirring. To ensure effective, efficient and through mixing of the materials, the tilt angle of the processing tool towards trailing direction enabled that tool shoulder held the stirred matrix by a cylindrical taper pin and this moved the composites material front to the back by the pin. The penetration rate of a pin depth as well as the tool shoulder radius when in contact with the workpiece is dictated by the pin length. In order to avoid defects in surface groove, inner channel, local thinning and excessive flash, it is then paramount to have better-designed pin profile to process the plates and ensure defects free. The calculation for the fractional volume, the area of the groove and the projected area of the tool pin is as shown in equation i to iii[19]. It worth mentioning that the processing parameters used were plunge depth, tilt angles, processing speed and rotational speed which respectively gave 0.3 mm, 3 °, 20 mm/min and 1500 rpm. Two passes on each process parameters in the same direction with the tool rotational movement with 100 % inter-pass overlap. The distribution of the double passes is 0.2 mm depth for first pass and 0.1 mm depth for the second pass with 100 % inter-pass overlap. A remarkable surface finish was achieved on each processed plate due to differentially selected processing parameters

$$Volume\ of\ Fraction = \frac{Area\ of\ groove}{Projected\ Area\ of\ tool\ pin}\ x\ 100 \quad (1)$$

$$Area\ of\ the\ groove = Groove\ width\ x\ Goove\ depth \quad (2)$$

$$Projected\ Area\ of the\ tool\ pin = Pin\ diameter\ x\ Pin\ length \quad (3)$$

Figure 2(a): NC-Controlled FSW

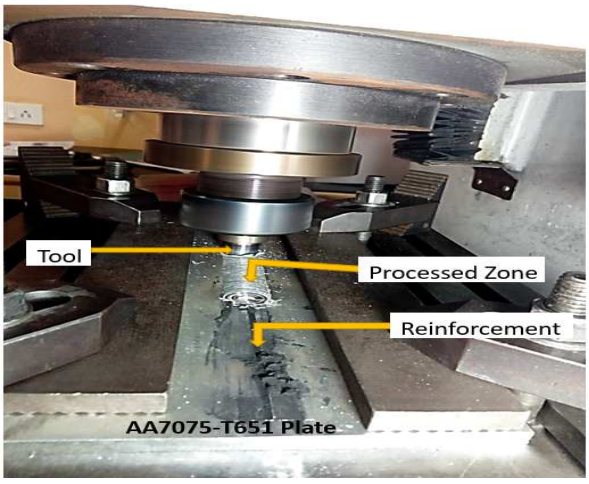

Figure 2(b): Processing Set Up

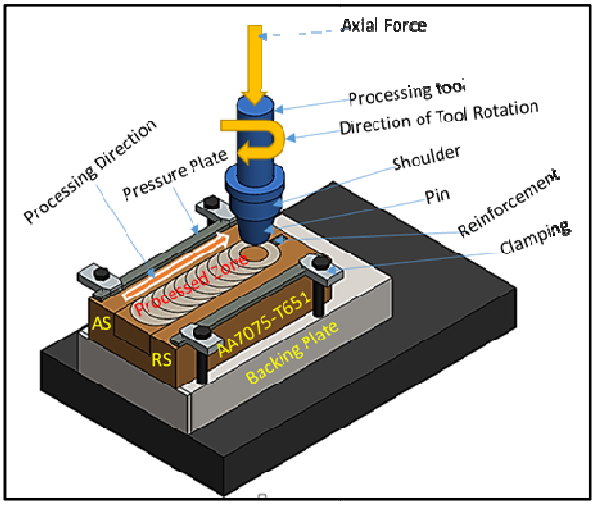

Figure 2(c): Schematic 3D Model of FSP

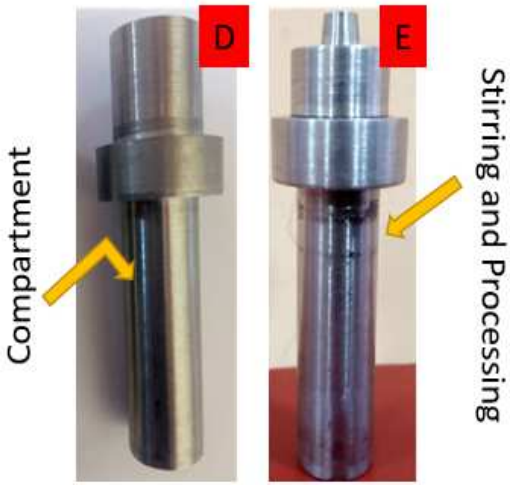

Figure 2(d) & (e): Pinless Tool & Tool with Pin

TENSILE TESTING

Tensile test specimens were prepared in conformance to the standard test requirement ASTM B557M-10. The tests samples were 6mm thickness is a substandard size of 100 mm long were cut to specification using waterjet cutter. Figure 3a shows the three dimensional model at different orientation of the test sample while Figure 3b shows the photograph images of the test samples before and after fracture had taken place. Figure 3c represents the X force P type of Zwick/Roell Z250 tensile testing machine which has the capacity of 250 kN force and 2mV/v characteristics. The data were acquired on testXpert II software installed on a PC. The tests were carried out on AA7075-T651/WFA-NPs, AA7075-T651/CFA-NPs, processed AA7075-T651 and unprocessed AA7075-T651. The tests were conducted in a triplicate and the average values were taken and recorded for plotting and analysis. The following parameters were recorded and evaluated the maximum stress value (R_m), the stress at 0.1 % offset strain ($R_{p0.1}$), Young Modulus (M_E), stress at 0.5 % offset strain ($R_{p0.5}$), stress-longitudinal plots, and the stress at 0.2 % offset strain ($R_{p0.2}$) as depicted in Figure 6.

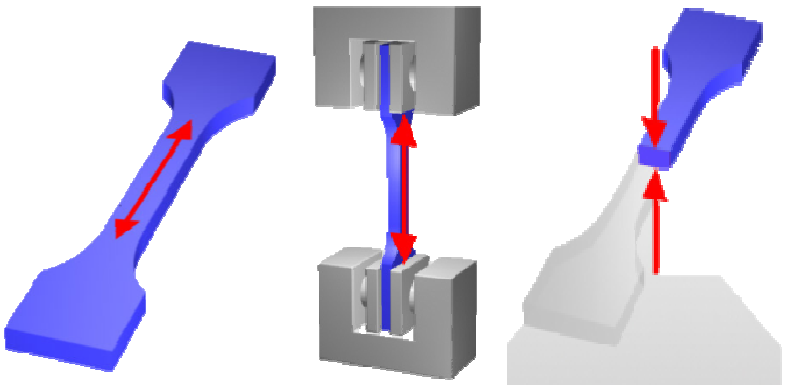

Figure 3(a): 3D Model of the Tensile Specimen used at Different Geometry

Figure 3(b): Macrograph of Tensile Test Specimen

Figure 3(c): Zwick/Roell Z250 Tensile Testing Machine

CORROSION TEST

Corrosion Sample Preparation

The percentage inhibition performance efficiency (%IPE) was conducted on friction stir processed aluminium alloy matrix composites of AA7075-T651/WFA-NPs and AA7075-T651/CFA-NPs. The corrosion test samples are in the dimensions 24 mm x 10 mm x 6 mm. The corrosion tests were also conducted on the unprocessed base metal (UBM) and processed base metal (PBM) without reinforcement to as control experiment 1and 2 respectively. The samples were prepared for corrosion test by grinding and polishing them in different grades of emery papers varying from 280, 350, 500, and 800 to 1200 grades and were well rinsed in sufficient distilled water. A corrosive medium containing 3.5 % NaCl solution to serve as seawater for the test.

Electrochemical Measurement

The electrochemical behaviours of the friction stir processed aluminium alloy matrix composites (AMC) containing the following samples tests AA7075-T651/WFA-NPs, AA7075-T651/CFA-NPs, PBM and UBM were examined by using open circuit potential (OCP) and potentiodynamic polarisation measurements were also carried out using Autolab PGSTAT 101 Metrohm potentiostat/galvanostat in which NOVA software 2.1.2 version was incorporated

and an electrochemical cell which has 3-electrode connections was used and the test was performed at an ambient temperature of 25°C containing 100 ml of 3.5 % NaCl solution as electrolyte. The working electrodes (WE) in this study were AA7075-T651/WFA-NPs, AA7075-T651/CFA-NPs, PBM and UBM; the counter electrode (CE) which is the auxiliary electrode in the study was graphite and the reference electrode (RE) was potassium chloride electrode (PCE). The potentiodynamic polarization plots were set at a cathodic potential of -1.5 V and anodic potential of 1.5 V against open circuit potential with 0.005 m/s sweep rate, i. e. scan rate. The working electrodes were individually immersed in the 3.54 % NaCl medium of electrolytes while the OCP of each WE were estimated in a span of 10 minutes and for a steady-state potential to be attained, at the same time potentiodynamic polarisation values were recorded after the OCP values were taken. To ensure and confirm reproducibility corrosion test was performed three times on each WE. The following data were extracted from the Tafel curves and recorded, polarization potential (Ecorr), current density (jcorr), while the percentage inhibition performance efficiency (IPE %) i.e. the percentage corrosion mitigation ability and the surface courage (□) were calculated using equations iv to v[20]–[23].

$$\theta = 1 - \frac{j_{corr}}{j_{0corr}} \tag{4}$$

$$IPE\ \% = 1 - \frac{j_{corr}}{j_{0corr}}\ x\ 100 \tag{5}$$

Where j_{corr} is the inhibited corrosion current densities and j_{ocorr} is the uninhibited corrosion current density.

RESULTS AND DISCUSSIONS

Characterizations of WFA-NPs and CFA-NPs

Morphological and physiological behaviours of FAs were carried using different tools to analyse them. The chemical composition of the FAs was carried out using X-Ray Fluorescence (XRF) spectroscopy (model PHILIP PW1404 XRF) Wavelength Disperse Spectrometer and the analysis of the investigation is as displayed in Table 3.

Table 3: The Chemical Composition of CFA-NPs and WFA-NPs

Chemical Formula	CFA (wt%)	WFA (wt%)
Al_2O_3	30.93	10.7
SiO_2	51.43	46.31
MgO	1.95	0.36
TiO_2	1.74	0.933
Fe_2O_3	2.29	17.28
CaO	6.75	3.002
MnO	0.02	-
MnO_2	-	0.0471
Na_2O	0.54	2.48
P_2O_3	1.08	-
P_2O_5	-	0.113
Cr_2O_3	0.77	-
K_2O	0.77	2.53
N_2O	0.01	-
SO_3	0.54	3.423
LOI	1.21	8
	Σ= 99.28	Σ= 87.17

The Scanning electron microscope (SEM) of model TESCAN and type VEGA 3 LMH coupled with Energy Dispersive Spectrometer (EDS) was employed for the morphological study of the FAs. Each sample was first sputter-

coated with a thin layer of carbon for conductivity and better resolution. The beam intensity and accelerating voltages are 12 and 20 kV respectively and all SEM Images were taken at 1000 x. The SEM Images for both FAs and their elemental compositions are depicted in Figure 4.

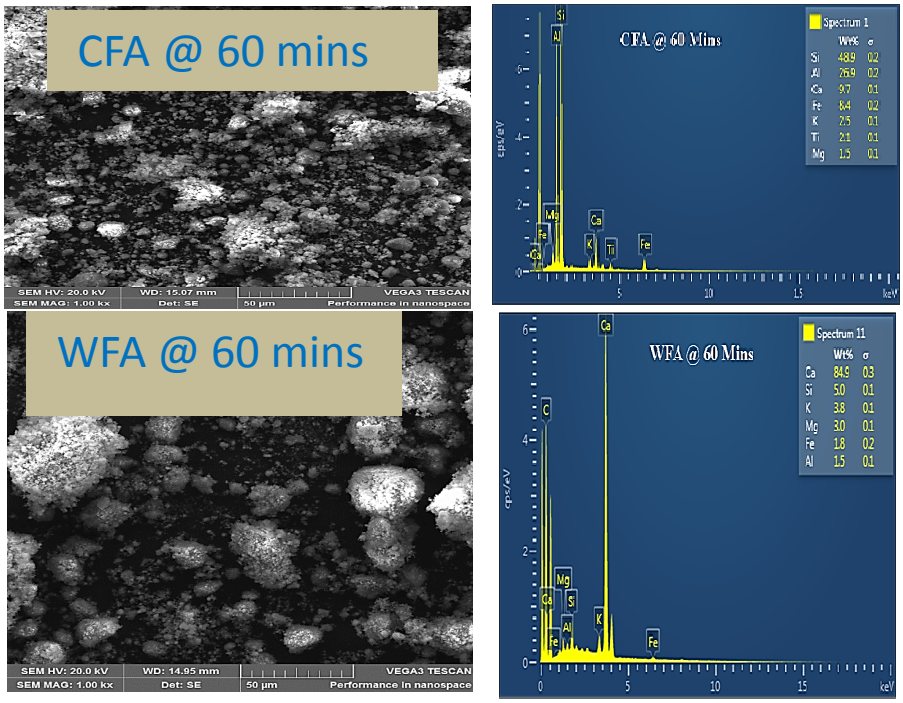

Figure 4: SEM Images and their Corresponding Energy Dispersive Spectrometer (EDS) for CFA and WFA

X-Ray Diffraction (XRD)

XRD analysis was carried out on the PHILIPS X'Pert (model number 12NC: 943003040601) with machine diffractometer operational parameters as shown in Table 4. The XRD test conducted was to confirm the mineralogical compositions and a crystal structure that are present in each FA sample. The XRD was acquired using copper Kα radiation (λ = 1.5406 Å)and kα radiation(λ = 1.39225 Å) and an automatic divergence slit; i. e., an irradiated sample length that is independent of the Bragg angles ((2θ) in degree). The diffraction patterns and crystal phases at different milling times were obtained. The diffractograms of both WFA and CFA is presented in Figure 5.

Table 4: Diffractometer Machine Operational Parametric Values

Property	Specification
Current	40mA
Excitation voltage	40kV
Scanning rate	0.05 (2□/seg)

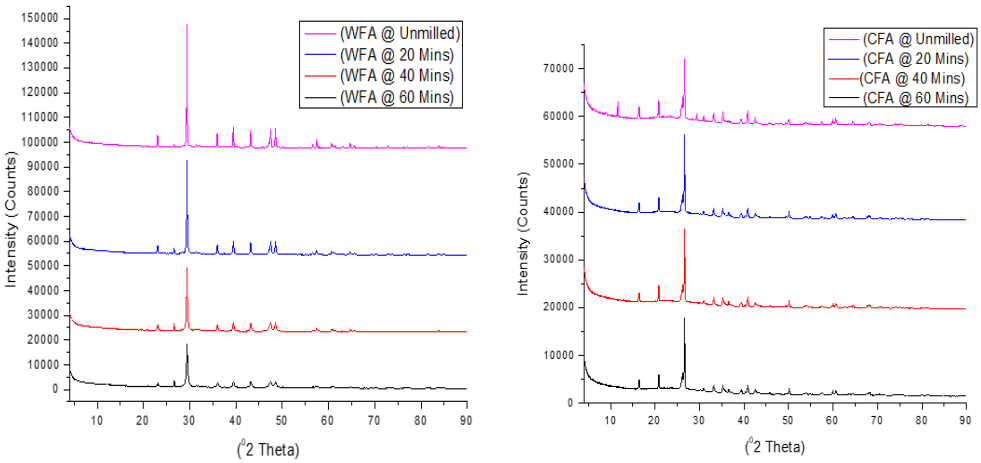

Figure 5: XRD Diffractograms of CFA-NPs & WFA-NPs at different Milling Time

In Figure 5, the intensity decreased with milling time for the WFA, which remained almost constant for CFA. Also, comparing the peak intensity of CFA with WFA, a higher value of count was observed at every stage of milling CFA. At almost 30° (2) CFA and 30° (2) WFA, the peaks were observed to higher. When considering, CFA, it was higher in 0 minutes and at 20, 40 and 60 minutes, the intensity maintained almost same peak, which dictates that there is the stability of quality in CFA while in WFA, 0 minutes proved to have the highest peak and there was a gradual reduction as the milling time increases. This reduction could be as a result of contaminations in WFA from the source of preparation or the nature of the timber or wood-fired to generate ash. Hence, the integrity of the CFA remained evenly and subjective of the fact that it is a suitable material (powder reinforcement and corrosion inhibitor) and with relative to its elemental composition; show in high percentage proportion of Al_2O_3 and less of Iron Oxides. The opposite is the case of WFA. The crystal phases detected by the XRD in WFA are rhombohedral, hexagonal, cubic and tetragonal while that of CFA are anorthic, orthorhombic, hexagonal, and rhombohedral. XRD analysis also revealed that the minerals that are dominated in wood fly ash are calcite ($CaC0_3$), quartz (SiO_2), Sylvite (KCl), Lime (CaO), maghemite-Q (γ-Fe_2O_3), nitratetine ($Na(NO_3)$) and magnetite (Fe_3O_4) while that of coal fly ash is Hematite (Fe_2O_3), Mullite ($Al_{2.32}Si_{0.68}O_{4.84}$), Sillimanite ($Al_2(SiO_4)O$, Quartz ($SiO_2$), Microcline ($KAlSi_3O_8$), Calcite high ($CaCO_3$),.

TENSILE TEST RESULTS

Table 5 shows the results of the tensile tests conducted on the fabricated matrix composites by the use of Xforce P type of Zwick/Roell Z250 tensile testing machine. The tests were conducted to evaluate the efficacy and potency of the reinforcement such as WFA-NPs as well CFA-NPs on tensile behaviour. The tests were carried out on fabricated matrix composites made up of AA7075-T651/WFA-NPs and also on the AA7075-T651/CFA-NPs aluminium matrix composites. The tests were done in triplicate and their average values were taken and recorded. The tests were being conducted on the processed base metal AA7075-T651 and unprocessed base material AA7075-T651 as both are serve as control experiments. The combine plots for all the test samples is represented in Figure 6.

Table 5: Tensile Results for AA7075-T651/WFA-NPs AMC, Unprocessed AA7075-T651, AA7075-T651/CFA-NPs AMC and Processed AA7075-T651

	m_E	R_m	F_m	$R_{p0.1}$	$R_{p0.2}$	$R_{p0.5}$	$R_{t0.5}$	$A_{t\ (corr.)}$
	GPa	MPa	kN	MPa	MPa	MPa	MPa	%
PBM (AA7075 - T651)	5.35351	362.9048	13.06457	213.24	228.2679	251.8613	7.607991	14.30768
UBM (AA7075-T651)	9.38165	620.9030	22.35251	559.0751	572.9528	588.4694	7.334991	9.732209
AA7075-T651/WFA-NPs	5.82818	367.8804	13.2437	223.6769	237.2417	260.1043	8.392041	14.63601
AA7075-T651/CFA-NPs	5.14402	367.7832	13.2402	241.9172	254.6327	277.3155	7.749521	14.19652

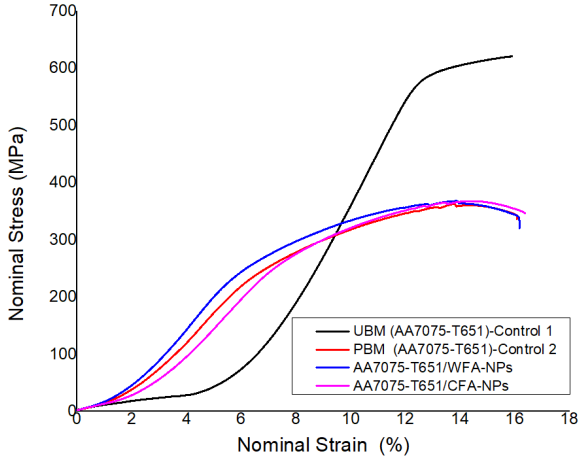

Figure 6: Nominal Stress Versus Nominal Strain for AA7075-T651/WFA-NPs AMC, Unprocessed AA7075-T651, AA7075-T651/CFA-NPs AMC and Processed AA7075-T651

Table 5presented the comparison tensile strength values on using coal fly ash and wood fly ash as reinforcement particles on high strength aluminium alloy 7075-T651 and the result is being compared with processing aluminium alloy 7075-T651 without reinforcement as control 2 and unprocessed aluminium alloy 7075-T651 as control 1. It can be deduced from Table 5that unprocessed base metal (UBM) which was control 1 has the highest ultimate tensile strength (R_m), breaking force (F_m), Modulus of Elasticity (M_E) and the stress at 0.2 % offset strain ($R_{p0.2}$) to be 620 MPa, 22.35251 KN, 9.38165 GPa, 237.2417 MPa respectively and also maintained its highest values in the case of stress at 0.1 % offset strain ($R_{p0.1}$) and the stress at 0.5 % offset strain ($R_{p0.5}$) for 559.051 MPa and 588.4696 MPa respectively.

It was observed in Table 5that processed base metal (PBM) of AA7075-T651 without reinforcement has the lowest values for ultimate tensile strength (R_m), breaking force (F_m), and the stress at 0.2 % offset strain ($R_{p0.2}$) as 362.9048 MPa, 13.06457 KN, and 228.2679 MPa respectively. Placing the tensile strength of friction stir processed of AA7075-T651/WFA-NPs and AA7075-T651-CFA-NPs matrix composites and at the same time compare the tensile values with the control experiments. It was observed that both matrix composites of AA7075-T651/CFA-NPs and AA7075-T651/WFA-NPs have relatively equal tensile strength values, the ultimate tensile strength (R_m) for AA7075-T651/WFA-NPs was 367.8804 MPa while that of AA7075-T651/CFA-NPs was 367.7832 MPa this was also evident in Figure 6. Both the AA7075-T651/CFA-NPs and AA7075-T651/WFA-NPs have a relatively equal number of breaking force (F_m) of 13.2402 and 13.2437 KN respectively which is slightlyhigher than that of PBM. Similar relative values for AA7075-T651/CFA-

NPs and AA7075-T651/WFA-NPs were recorded in Modulus of Elasticity (M_E) and the stress at 0.2 % offset strain ($R_{p0.2}$) which are 5.14402 and 5.82818 respectively which are also close to the value of PBM. The reinforcement of AA7075-T651 with nanoparticles of WFA and CFA has no significant effects on the tensile strength of aluminium alloy 7075-T651 when compared with processed base metal – AA7075-T651 without reinforcement as they all have extremely close values for tensile data which was also predicted in stress vs strain curves depicted in Figure 6.

Corrosion Mitigation Assessments

Pitting Corrosion

Pit corrosion attack is the type of corrosion that occur in the presence of aggressive, vigorous and active chlorine ions [24]. Crack initiation during pitting attacks usually occur at the weakest sites in the oxides as a result of the violet and effective chlorine attack. Equations vi–ix presents chemical equation for the illustration pit propagation[25].

$$Al \rightarrow Al^3 + 3e^- \quad (6)$$

$$Al + 3H_2O \rightarrow Al(OH)_3 + 3H^+ \quad (7)$$

The most crucial reduction procedures is the reduction of oxygen in the reaction and the evolution of hydrogen at the metallic cathodes

$$2H^+ + 2e \rightarrow H_2 \quad (8)$$

$$O_2 + 2H_2O + 4e \quad (9)$$

It was observed that increase in the pits propagations changes the anodic pit environment.

Tafel Polarization Test

The Tafel polarization tests were used to measure the degree of pitting corrosion resistance. The nugget area of the processed test samples such as AA7075-T651/WFA-NPs, AA7075-T651/CFA-NPs and processed AA7075-T651 without reinforcement as well as unprocessed base metal AA7075-T651 were all exposed to 3.5 % NaCl medium for the determination of anodic polarization plots. The value of corrosion rate (CR), corrosion density (i_{corr}), anodic slope (ba), polarization resistance (PR), corrosion potential (E_{corr}), and cathodic slope (bc) were derived by interpolating cathodic and anodic tafel plots in the presence and absence of reinforcement inhibitors as shown in Table 6 and Figure 8 while Equation 5 was employed to evaluate percentage inhibition efficiency (IE %). The corresponding values for OCP has been presented in Table 6 and Figure 7 which reveals that polarization has taken place by combine integrated effects of anodic and cathodic branches. It can be deduced from experimental results that corrosion protection rate is influenced by the presence of inhibitors which greatly reduced corrosion rate and there exists in the cathodic and anodic polarization plots a migration in the values of corrosion rate towards the current densities. Evolution of cathodic reaction and dissolution of anodic reactions in the matrix of aluminium alloy are hindered by this migration [22], [26], [27].

Table 6: Potentiodynamic Polarization for AA7075-T651/WFA-NPs AMC, Unprocessed AA7075-T651, AA7075-T651/CFA-NPs AMC and Processed AA7075-T651 in 3.5% NaCl Medium at 25 °C Ambient Temperature

	Corrosion Potential	Corrosion Rate	Corrosion Current	Open Circuit Potential	Polarization Resistance	Anodic Tafel Slope	Cathodic Tafel Slope	% Inhibition performance Efficiency
Samples	**E_{corr} (mV)**	**Cr (mm/year)**	**j_{corr} (µA/cm^2)**	**OCP (V)**	**Pr (Ω)**	**|ba| (mV/dec)**	**|bc| (mV/dec)**	**% IPE**
Control 1 (UBM)	-1425.8	5.0718	436	-0.96954	98.597	169.62	238.31	0
Control 2 (PBM)	-1424	1.829	157	-1.00922	178.14	88.564	238.24	63.99
AA7075-T651/CFA-NPs	-1450.2	0.8241	70.9	-0.99152	417.28	108.3	183.77	83.74
AA7075-T651/WFA-NPs	-1230.7	0.12068	10.4	-1.0318	776.22	56.228	27.71	97.61

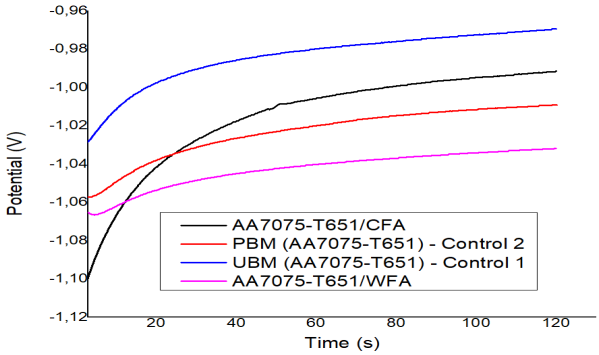

Figure 7: Evolution of Open Circuit Potential (OCP) vs. Exposure Time for AA7075-T651/WFA-NPs AMC, Unprocessed AA7075-T651, AA7075-T651/CFA-NPs AMC and Processed AA7075-T651 in 3.5% NaCl Solution at Ambient Temperature of 25 °C

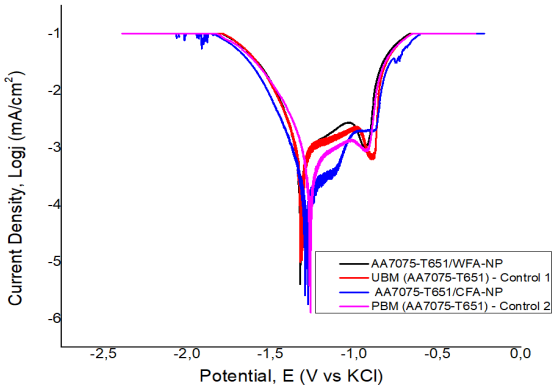

Figure 8: Tafel Potentiodynamic Polarization Curves for AA7075-T651/WFA-NPs AMC, Unprocessed AA7075-T651, AA7075-T651/CFA-NPs AMC and Processed AA7075-T651 in 3.5% NaCl Solution at 25 °C Ambient Temperature

The percentage inhibition performance efficiency (% IPE) was calculated with Equation 5 above and the results of the evaluation and the data extracted from Tafel graphs and OCP is presented in Table 6. It can be deduced from Table

6that matrix composites AA7075-T651/WFA-NPs exhibits the highest corrosion protection performance with % IPE of 97.61 % as against AA7075-T651/CFA-NPs corrosion protection performance efficiency with %IPE of 83.74 %. This trend was also manifested in the values of corrosion rate for AA7075-T651/WFA-NPs and AA7075-T651/CFA-NPs which are 0.12068 and 0.8241 mm/year and with polarization resistances of 776.22 Ω and 417.28 Ω respectively. The two matrix composites under investigations performed far better than the control experiments. Control 1 which was untreated base metal (UBM) and has been taken as reference point of study with corrosion rate of 5.0718 mm/year and polarization resistance of 98.597 Ω while control experiment 2 which was processed or treated base metal (PBM) without reinforcement has a corrosion rate of 1.829 mm/year which is very close to the value got for AA7075-T651/CFA-NPs and its polarization resistance was 178.14 Ω with a % IPE of 63.9 %. The trend observed in Table 6 was also supported by Figures 7 and 8. In general, one could see that reinforcement with wood fly ash nanoparticles in friction stir processing resists corrosion attack than coal fly ash nanoparticles under the same environmental corrosion mitigation medium. The shift in the negative trends of the corrosion potential values (E_{corr}) suggests potency of cathodic protection of the processing technique and the reinforcement applied.

CONCLUSIONS

From the experimental procedures, results and conclusions, the following assertions can be made:

- The Investigations reveals an excellent performance of wood fly ash nanoparticles when used for reinforcement and corrosion inhibition in friction stir processed AA7075-T651 when immersed in 3.5 % NaCl medium in ambient temperature by potentiodynamic polarization method.
- Aluminium 7075-T651 alloy Metal Matrix composites reinforced with wood fly ash exhibits the largest percentage of inhibition performance efficiency (%IPE) with a value of 97.61 % and that of coal fly ash inhibitive reinforcement particle has % IPE of 83.74 which also shows high corrosion protection has compared to PBM-control 2.
- It can be inferred from the results that AA7075-T61/WFA-NPs has an outstanding corrosion reduction rate which got reduced from the corrosion rate of unprocessed base metal AA7075-T651 which was observed to be 5.0718 mm/year to that made of AA7075-T61/WFA-NPs matrix composites which was 0.12068 mm/year.
- It can be concluded that the higher the polarization resistance the better the rate of corrosion protection, AA7075-T61/WFA-NPs aluminium matrix which had the lowest corrosion rate at the same time highest polarization resistance which are 0.12068 mm/year and 776.22 Ω respectively with a reduction in amount of current density which is 10.4 $\mu A/cm^2$.
- The unprocessed and untreated base metal (UBM) – control 1 has the highest tensile strength of 620.9030 MPa with breaking force of 22.35251 KN and highest elastic modulus of 9.38165 GPa among others. UBM isproved to have exceptional tensile strength behavioural characteristics.
- It was revealed that tensile strength values when AA7075-T651 was reinforced with WFA-NPs and CFA-NPs are very close which was 367.8804 and 367.7832 MPa, this was also observed to be in a close range with procced base metal (PBM) –control 2 which has a tensile strength of 362.9048 MPa. By this, it can be deduced that FAs nanoparticles have no significant influence of the reinforcement of friction stir processed AA7075-T651.

Appreciation

We want to sincerely thank the Chairman of Friction Stir Welding Laboratory, Prof. S. K. Pal for the permission granted to us to work on the friction stir welding machine at the Indian Institute of Technology (IIT) Kharagpur, India; Also, Dr. O. S. I. Fayomi, the Head of Surface Engineering Research Centre, Covenant University, Ota, Nigeria, for the permission to work on corrosion testing equipment; To the management of Material and Metallurgical Laboratory, Department of Mechanical Engineering Science, University of Johannesburg, South Africa where the tensile tests were conducted and also the University of Johannesburg, South Africa for the research trip support to India.

Conflict of Interest

The authors declared that there is no known conflict of interests

REFERENCES

1. *O. M. Ikumapayi, E. T. Akinlabi, and J. D. Majumdar, "Review on thermal, thermo- mechanical and thermal stress distribution during friction stir welding," Int. J. Mech. Eng. Technol., vol. 9, no. 8, pp. 534–548, 2018.*
2. *Krishnaja Devireddy et al., "Analysis of the Influence of Friction Stir processing on Gas Tungsten Arc Welding of 2024 Aluminum Alloy Weld Zone," Int. J. Mech. Prod. Eng. Res. Dev., vol. 8, no. 1, pp. 243–252, 2018.*
3. *A. Cerit, M. B. Karamiş, N. Fehmi, and Y. Kemal, "Effect of reinforcement particle size and volume fraction on wear behaviour of metal matrix composites," Tribol. Ind., vol. 30, no. 3–4, pp. 31–36, 2008.*
4. *D. N. Sun and Apelian, "Friction Stir Processing of Aluminum Cast Alloys for High Performance Applications," Alum. Form., pp. 44–50, 2011.*
5. *Sudhakar. M; Srinivasa Rao. CH; Meera Saheb. K, "Production of Surface Composites by Friction Stir Processing," Mater. Today Proc., vol. 5, no. 1, pp. 929–935, 2018.*
6. *Bawdekar and S. Singh, "Surface hardening and microstructural evolution of high carbon steel by friction stir processing," Int. J. Mech. Prod. Eng. Res. Dev., vol. 7, no. 3, pp. 343–354, 2017.*
7. *Dinaharan, "Influence of ceramic particulate type on microstructure and tensile strength of aluminum matrix composites produced using friction stir processing," J. Asian Ceram. Soc., vol. 4, no. 2, pp. 209–218, 2016.*
8. *P. M. Kumar and S. Jerome, "Effect Of Eccentricity Pin Geometry On The Fabrication Of Surface Composite (Al6061-T6 /Sic) By Friction Stir Processing," Int. J. Mech. Prod. Eng. Res. Dev., vol. 8, no. 6, pp. 249–254, 2018.*
9. *O. Sanusi and E. T. Akinlabi, "Friction-stir processing of a composite aluminium alloy (AA 1050) reinforced with titanium carbide powder," Mater. Tehnol., vol. 51, no. 3, pp. 427–435, 2017.*
10. *N. Fatchurrohman, N. Farhana, and C. D. Marini, "Investigation on the effect of Friction Stir Processing Parameters on Micro-structure and Micro-hardness of Rice Husk Ash reinforced Al6061 Metal Matrix Composites," IOP Conf. Ser. Mater. Sci. Eng., vol. 319, no. 1, pp. 0–6, 2018.*
11. *Y. X. Gan, D. Solomon, and M. Reinbolt, "Friction stir processing of particle reinforced composite materials," Materials (Basel)., vol. 3, no. 1, pp. 329–350, 2010.*
12. *S. A. Afolalu, A. A. Abioye, M. O. Udo, O. R. Adetunji, O. M. Ikumapayi, and S. B. Adejuyigbe, "Data showing the effects of temperature and time variances on nano-additives treatment of mild steel during machining," Data Br., vol. 19, pp. 456–461, 2018.*

13. Kumar, R., Pedgopu, V., Kumar, Anil., Thakur, Robin., & Pundir, Anil. (2013). CFD based analysis heat transfer and friction characteristics of broken multiple rib roughened solar air heater duct. Int J Mech Prod Eng Res Dev, 3, 165-172.

14. A. Daniyan, A. M. Omokhuale, A. A. Aderoba, O. M. Ikumapayi, and B. A. Adaramola, "Development and performance evaluation of organic fertilizer machinery," Cogent Eng., vol. 8, no. 1, pp. 1–22, 2017.

15. H. Rana, V. Badheka, A. Kumar, and A. Satyaprasad, "Strategical parametric investigation on manufacturing of Al–Mg–Zn–Cu alloy surface composites using FSP," Mater. Manuf. Process., vol. 33, no. 5, pp. 534–545, 2018

16. Sert and O. N. Celik, "Wear behavior of SiC-reinforced surface composite Al7075-T651 aluminum alloy produced using friction stir processing," Indian J. Eng. Mater. Sci., vol. 21, no. February, pp. 35–43, 2014.

17. P. Loganathan, A. Gnanavelbabu, and K. Rajkumar, "Analysis and characterization of friction behaviour on AA7075 / ZrB 2 composite under dry sliding condition Analysis and characterization of friction behaviour on AA7075 / ZrB 2 composite under dry sliding condition," Mater. Res. Express, vol. 6, pp. 1–14, 2019.

18. S. Joyson, A. Isaac, D. Jebaraj, D. Raja, S. Esther, and T. Akinlabi, "Microstructural Characterization and Tensile Behavior of Rutile (TiO2) - Microstructural Characterization and Tensile Behavior of Rutile (TiO 2) - Reinforced AA6063 Aluminum Matrix Composites Prepared by Friction Stir Processing," Acta Metall. Sin. (English Lett., no. August, pp. 1–12, 2018.

19. G. Akande, O. O. Oluwole, and O. S. I. Fayomi, "Optimizing the defensive characteristics of mild steel via the electrodeposition of Zn–Si3N4 reinforcing particles," Def. Technol., no. xxxx, pp. 1–7, 2018.

20. O. S. I. Fayomi and I. G. Akande, "Corrosion Mitigation of Aluminium in 3. 65 % NaCl Medium Using Hexamine," J. Bio-Tribo-Corrosion, vol. 5, no. 23, p. 0, 2019.

21. H. Gerengi, M. M. Solomon, F. E. Bagci, and E. J. Abai, "An evaluation of the anticorrosion e ff ect of ethylene glycol for AA7075-T6 alloy in 3. 5 % NaCl solution," Measurement, vol. 116, no. November 2018, pp. 264–272, 2018.

22. D. Mantha and S. A. Fawaz, "Standardized Test Method for Corrosion Pit-to-Fatigue Crack Transition for AA7075-T651 Aluminum Alloy," Adv. Mater. Res., vol. 891–892, pp. 205–210, 2014.

23. Yadav, D., & Gaikwad, A. (2015). Comparison and testing of tensile strength for low & medium carbon steel. International Journal of Mechanical Engineering (IJME), 4(5), 1-8.

24. D. Raguraman, D. Muruganandam, and L. K. K. Dhas, "Corrosion study in friction stir welded plates of AA6061 and AA7075," Int. J. ChemTech Res., vol. 6, no. 4, pp. 2577–2582, 2014.

25. Y. Liu and J. M. C. M. G. C. A. M. Janssen, "Combined Corrosion and Wear of Aluminium Alloy 7075-T6," J. Bio- Tribo-Corrosion, vol. 2, no. 2, pp. 1–7, 2016.

26. O. D. L. El, G. O. Hamed, and S. J. A. El, "Anticorrosive Formulation Based of the Epoxy Resin – Polyaminoamide Containing Zinc Phosphate Inhibitive Pigment Applied on Sulfo- Tartaric Anodized AA 7075-T6 in NaCl Medium," J. Bio-Tribo-Corrosion, vol. 5, no. 25, pp. 1–9, 2019.